

# Supporting Information

## **High-flux organic solvent nanofiltration membrane with binaphthol-based rigid-flexible microporous structures**

Wenming Fu, Wei Zhang, Haonan Chen, Shao-Lu Li\*, Wenxiong Shi\*, Yunxia Hu\*

State Key Laboratory of Separation Membranes and Membrane Processes, School of Materials Science and Engineering, Tiangong University, Tianjin 300387, P.R. China

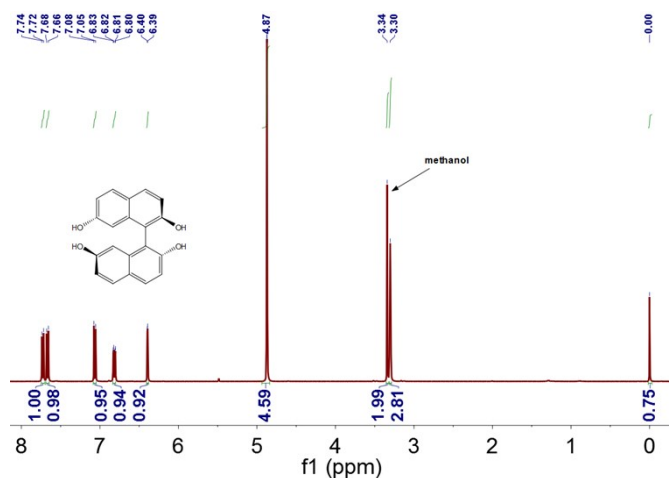
\* Corresponding authors:

Tel: +86-22-83955826, e-mail: [lishaolu@tiangong.edu.cn](mailto:lishaolu@tiangong.edu.cn) (S.-L. Li)

Tel: +86-22-83955822, e-mail: [wxshi@tiangong.edu.cn](mailto:wxshi@tiangong.edu.cn) (W. Shi)

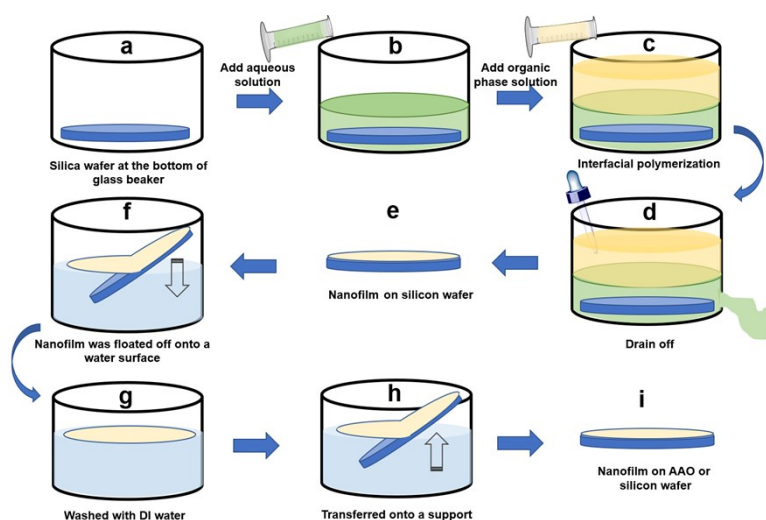
Tel: +86-22-83955129, e-mail: [yunxiah@tiangong.edu.cn](mailto:yunxiah@tiangong.edu.cn) (Y. Hu)

## Supplementary Figures



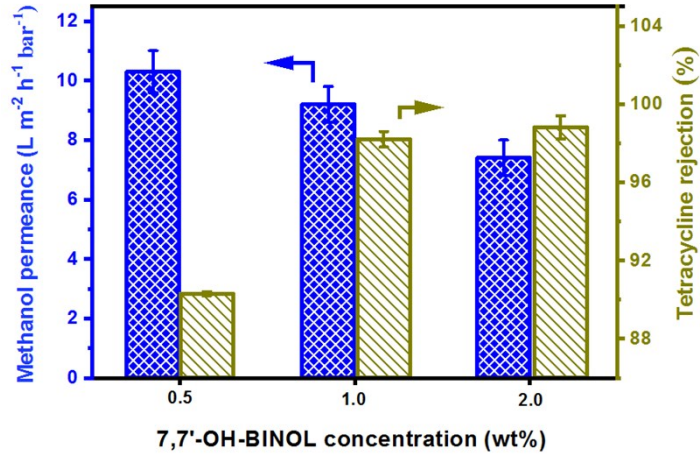
**Fig. S1.** <sup>1</sup>H NMR spectrum of 7,7'-OH-BINOL. <sup>1</sup>H NMR (400 MHz, Methanol-*d*<sub>4</sub>) δ 7.73 (d, *J* = 8.8 Hz, 1H), 7.67 (d, *J* = 8.8 Hz, 1H), 7.06 (d, *J* = 8.8 Hz, 1H), 6.82 (dd, *J* = 8.8, 2.4 Hz, 1H), 6.39 (d, *J* = 2.4 Hz, 1H), 4.87 (s, 5H), 3.34 (s, 2H), 3.30 (p, *J* = 1.6 Hz, 3H), -0.00 (s, 1H).

As shown in **Fig. S2**, the freestanding PAR-BINOL nanofilm was fabricated at an aqueous–organic interfacial polymerization in bulk and transferred onto supports. Briefly, the aqueous solution was poured into a glass beaker. Then, the TMC solution in Isopar G was gently added into the above beaker and the reaction time was 2 min. After that, the two immiscible solutions were drained off to obtain the freestanding nanofilm. Upon rinsing with DI water, the nanofilm was transferred onto anodized aluminum oxide (AAO) support or silicon wafer for further characterizations.

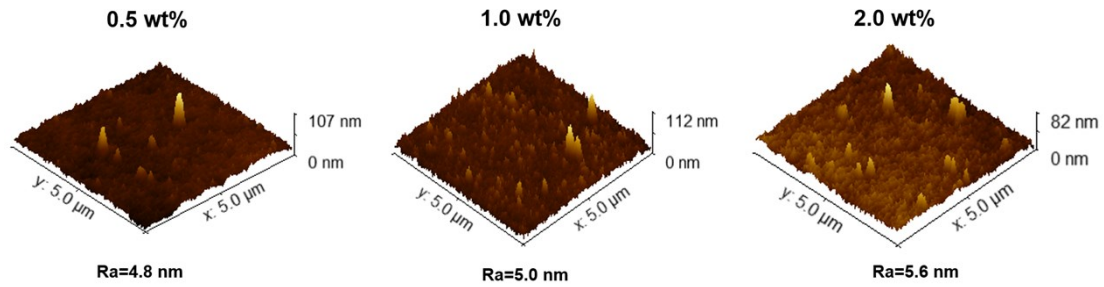


**Fig. S2.** Schematic illustration of the freestanding PAR-BINOL nanofilm fabricated at an aqueous–organic interfacial polymerization in bulk and transferred onto supports. a) Silica wafer at the bottom of glass beaker. b, c) the formation of PAR-BINOL nanofilm at the interface between an aqueous phase containing 7,7'-OH-BINOL and an Isopar G phase containing TMC. d, e) The PAR-BINOL nanofilm was deposited on the silica wafer by decreasing the interface. f, g) The PAR-BINOL nanofilm was floated off onto a water surface and washed with DI water. h) Silica wafer or AAO touched the PAR-BINOL nanofilm at the water surface. i) The PAR-BINOL nanofilm with top surface upwards was air-dried for further characterization.

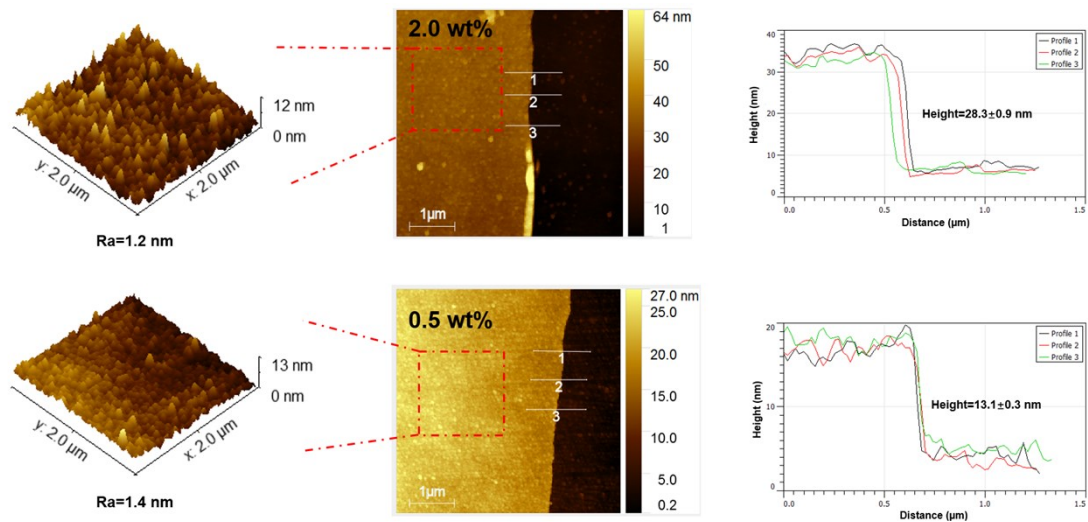
As shown in **Fig. S3**, as the monomer concentration of 7,7'-OH-BINOL was increased from 0.5 wt% to 1.0 wt%, the membrane rejection towards tetracycline (TC) increased from 90.3% to 98.2%, and the methanol permeability coefficient merely decreased from  $10.3 \text{ L m}^{-2} \text{ h}^{-1} \text{ bar}^{-1}$  to  $9.2 \text{ L m}^{-2} \text{ h}^{-1} \text{ bar}^{-1}$ . Further increasing the monomer concentration to 2.0 wt%, the TC rejection increased slightly to 98.8%, but the methanol permeability coefficient decreased from  $9.2 \text{ L m}^{-2} \text{ h}^{-1} \text{ bar}^{-1}$  to  $7.4 \text{ L m}^{-2} \text{ h}^{-1} \text{ bar}^{-1}$ . Thus, we choose the monomer concentration of 1.0 wt% 7,7'-OH-BINOL to prepare the PAR-BINOL membrane. As revealed in **Fig. S4** and **Fig. S5**, the surface roughness of these membranes varied little (the value of  $R_a$  is about 5 nm), and the thickness of these nanofilms increased from 13 nm to 28 nm with increasing monomer concentration. All of the prepared PAR-BINOL membranes were integral and continuous. The change in membrane performance may be due to the increase of membrane thickness with the increasing monomer concentration.<sup>1-3</sup>



**Fig. S3.** Effect of the 7,7'-OH-BINOL concentration on the separation performances of the prepared PAR-BINOL membranes.

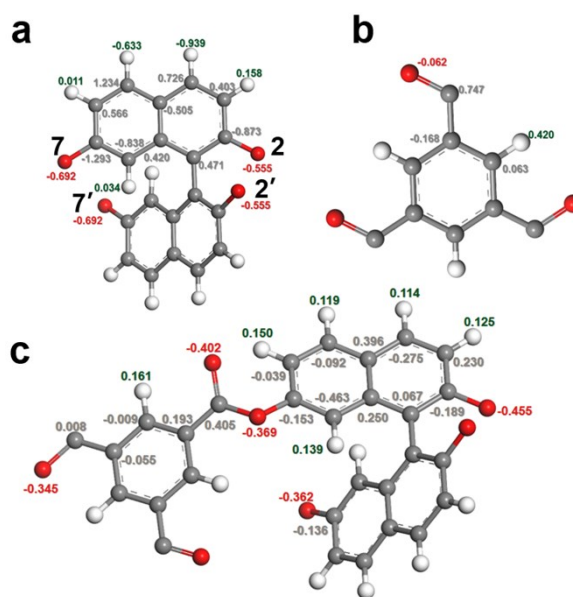


**Fig. S4.** 3D AFM images of the PAR-BINOL membranes prepared on the XP84 UF support when increasing the 7,7'-OH-BINOL monomer concentration from 0.5 wt% and 1.0 wt%, to 2.0 wt% during interfacial polymerization.

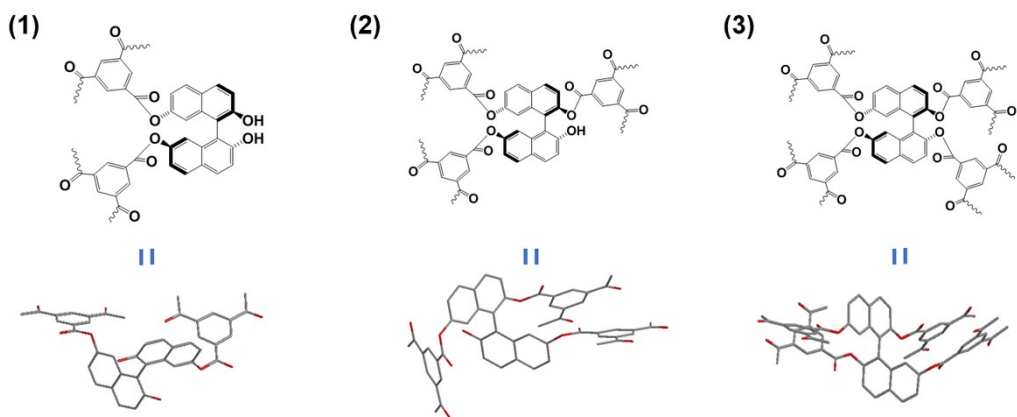


**Fig. S5.** 2D/3D AFM images and height profiles of the freestanding PAR-BINOL nanofilms prepared using 2.0 wt% and 0.5 wt% 7,7'-OH-BINOL during interfacial polymerization.

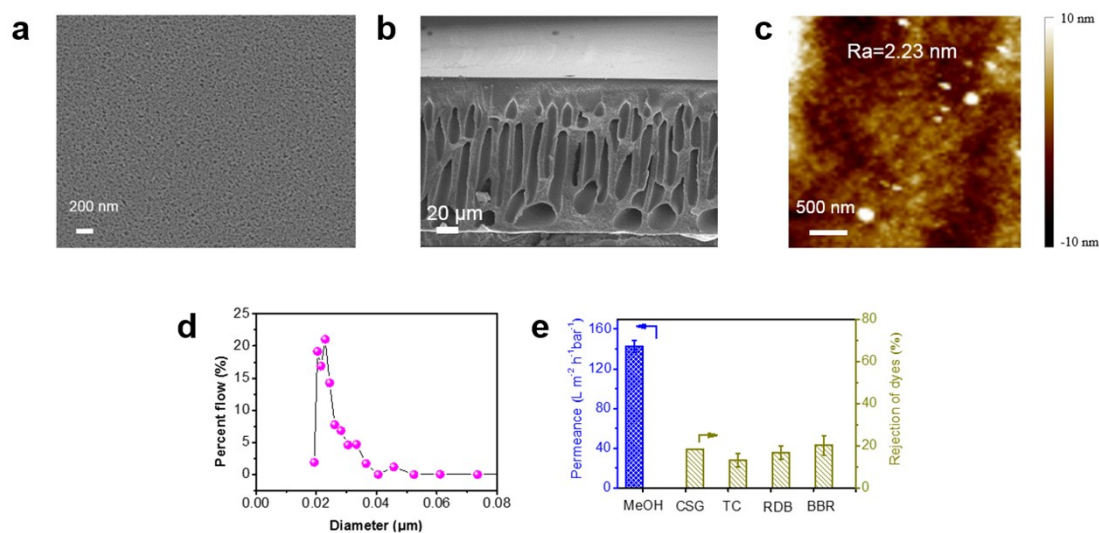
As shown in **Fig. S6**, the 7,7'-OH has more negative charge than 2,2'-OH, where, the charge of the oxygen atom reflects its nucleophilicity during the reaction process. This result means that the 7,7'-OH is more vulnerable to attack by nucleophiles, indicating that 7,7'-OH has higher reactivity than the 2,2'-OH part. Therefore, it suggests that the reaction of 7,7'-OH-BINOL and TMC occurs preferentially at the 7,7'-OH substitution position, followed by the 2,2'-OH substitution position. The proposed chemical structures of the PAR-BINOL network formed through the interfacial polymerization of 7,7'-OH-BINOL and TMC is shown in **Fig. S7**.



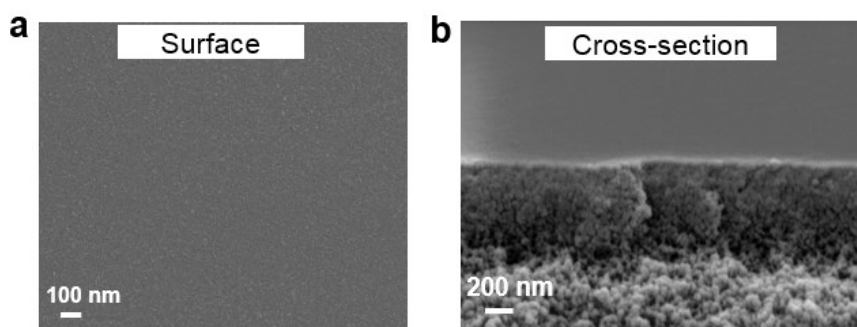
**Fig. S6.** Chemical structures and partial charges of (a) 7,7'-OH-BINOL, (b) TMC and (c) the dimer performed using the B3LYP method with 6-31+g(d, p) basis sets by Gaussian 09 code.<sup>4, 5, 6</sup>



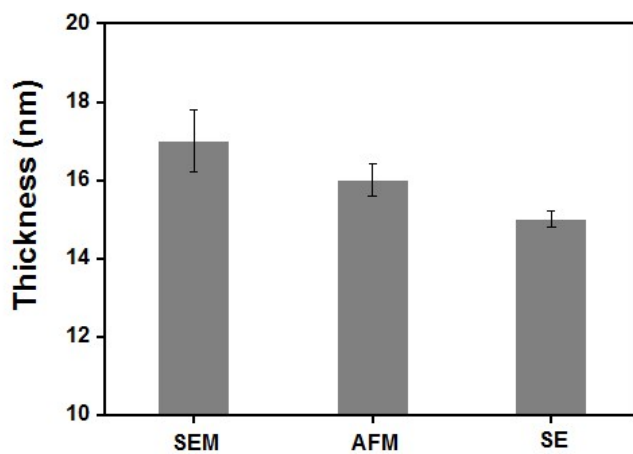
**Fig. S7.** The proposed chemical structures of the PAR-BINOL network formed through the interfacial polymerization of 7,7'-OH-BINOL and TMC.



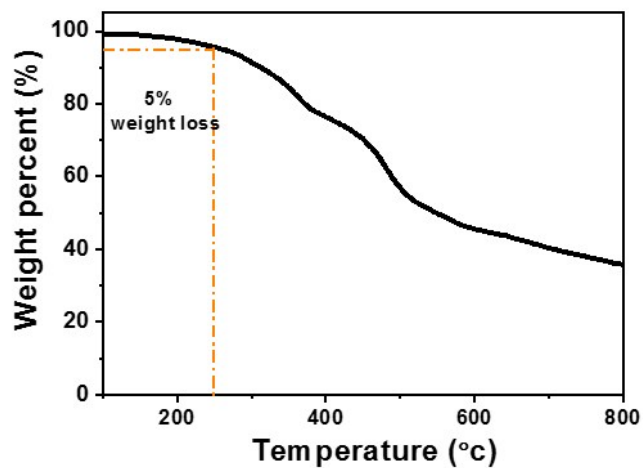
**Fig. S8.** Morphology, structures and separation performances of the XP84 UF support prepared *via* phase inversion. (a) Surface SEM image and (b) Cross-sectional SEM image and (c) 3×3 μm<sup>2</sup> AFM image. (d) Pore size distribution, (e) methanol permeance and dye rejections of the XP84 UF support towards BBR, RDB, TC and CSG in methanol.



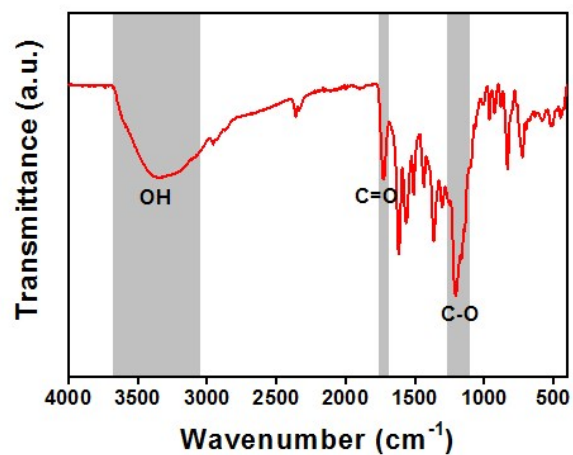
**Fig. S9.** (a) Surface and (b) cross-sectional SEM images of the PAR-BINOL membrane formed on the XP84 UF support.



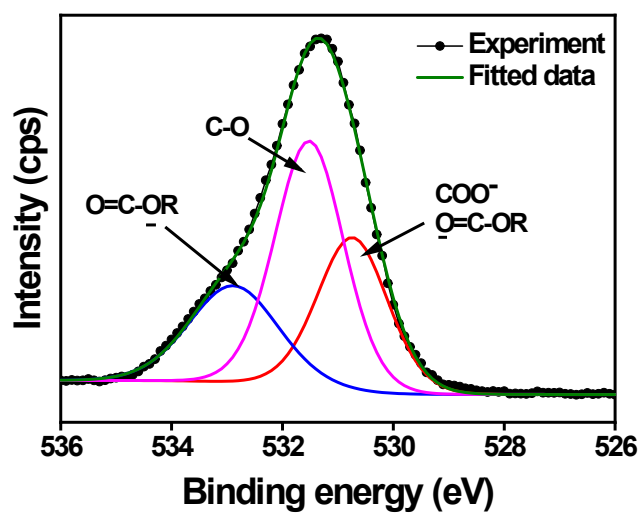
**Fig. S10.** The thickness of the PAR-BINOL nanofilm obtained by SEM, AFM and SE.



**Fig. S11.** The thermal gravimetric curve of the PAR-BINOL polymer solid.

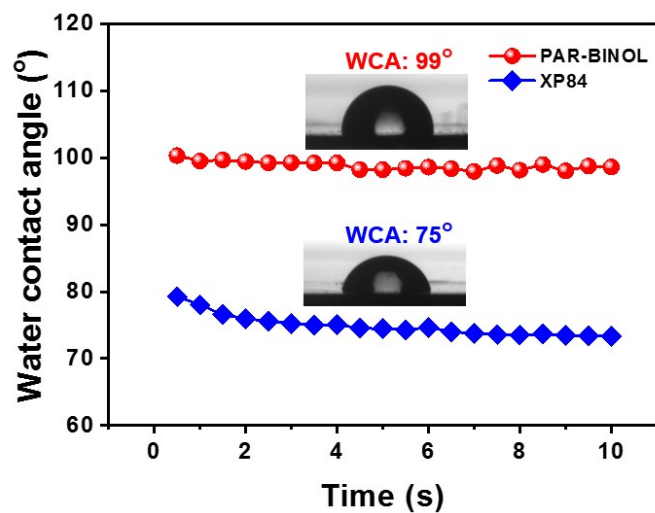


**Fig. S12.** The FTIR spectra of the PAR-BINOL polymer solid.

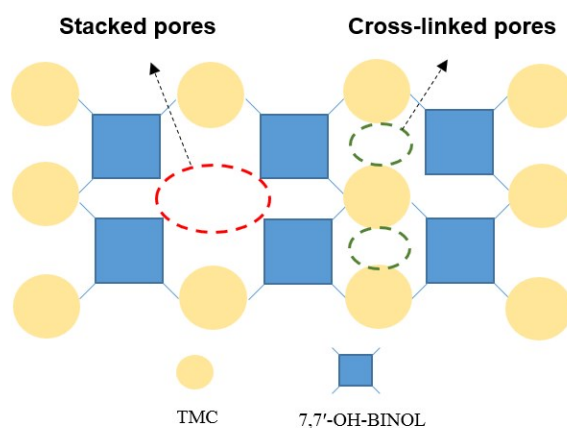


**Fig. S13.** The deconvolution O1s peak obtained from the high-resolution XPS spectra of the PAR-BINOL membrane.

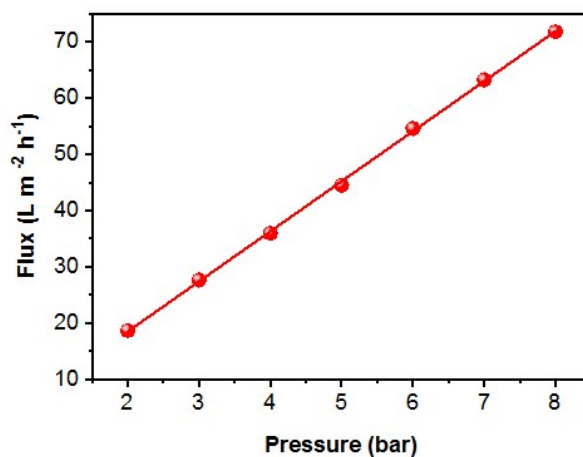




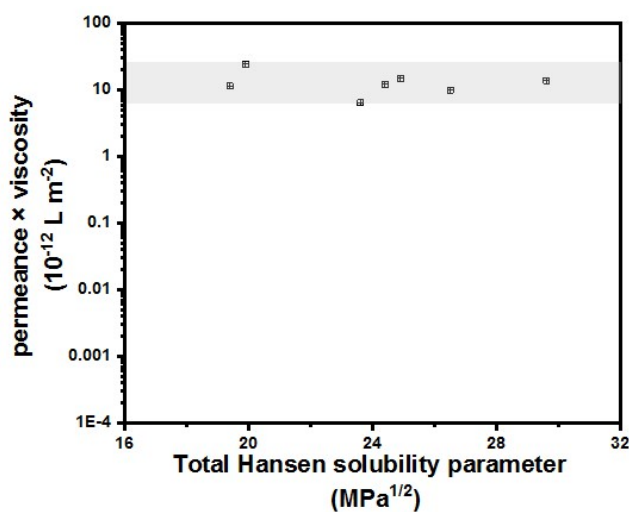
**Fig. S14.** The dynamic water contact angles of the PAR-BINOL membrane and the XP84 UF support.



**Fig. S15.** Schematic representation of possible pore formation of stacked and cross-linked pores in the PAR-BINOL membrane.

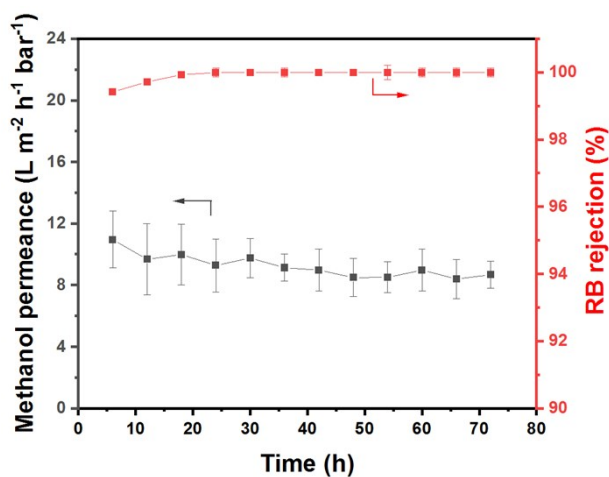


**Fig. S16.** Linear increase of methanol flux of the PAR-BINOL membrane with applied pressure.



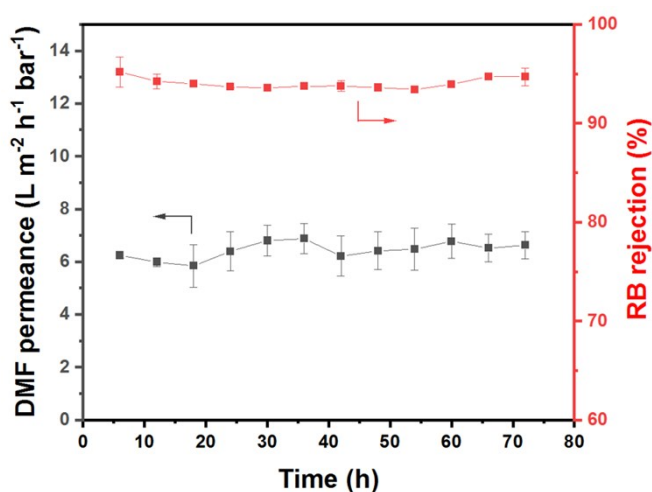
**Fig. S17.** Product of permeance and viscosity of solvent as a function of total Hansen solubility parameter for PAR-BINOL membrane.

As shown in **Fig. S18**, the methanol permeance remained at  $8.7 \text{ L m}^{-2} \text{ h}^{-1} \text{ bar}^{-1}$  and the RB rejection remained at about 99.9% during a 72 h test, indicating the long-term stable separation performance of the fabricated OSN membranes.



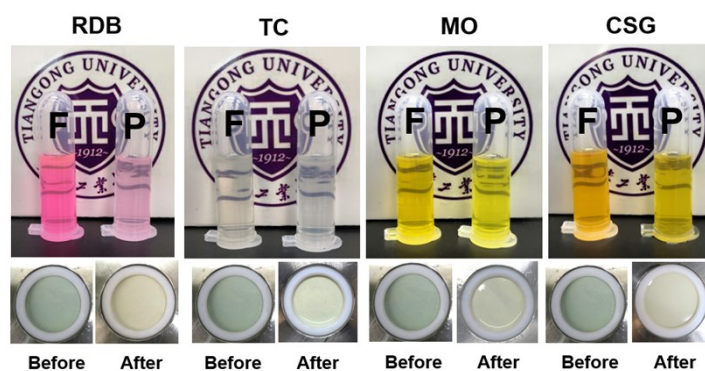
**Fig. S18.** The long-term performance of the PAR-BINOL membrane using 50 ppm RB/methanol solution as feed. Measurements were conducted in a dead-end cell with a volume of 220 mL at  $23\pm 0.5$  °C. The stirring speed was set to 600 rpm to minimize the potential concentration polarization. The permeate was poured back into the dead-end cell per hour to ensure the stability of the feed concentration.

As shown in **Fig. S19**, the DMF permeance remained at  $6.6 \text{ L m}^{-2} \text{ h}^{-1} \text{ bar}^{-1}$  and the RB rejection remained at  $\sim 95\%$  during a 72 h test, indicating the super resistance of the fabricated OSN membranes to strong polar DMF.



**Fig. S19.** The long-term performance of the PAR-BINOL membrane using 50 ppm RB/DMF solution as feed. Measurements were conducted in a dead-end cell with a volume of 220 mL at  $23\pm 0.5$  °C. The stirring speed was set to 600 rpm to minimize the potential concentration polarization. The permeate was poured back into the dead-end cell per hour to ensure the stability

of the feed concentration.



**Fig. S20.** Photographs of solutions of feed (F) and permeate (P) containing different dye molecules in methanol after organic solvent nanofiltration. The visual images of membrane appearances before and after filtration experiments shown at the bottom of the photographs. The dyes dissolved in methanol include: Rhodamine B (RDB,  $M_w = 479 \text{ g mol}^{-1}$ ), Tetracycline (TC,  $M_w = 444 \text{ g mol}^{-1}$ ), Methyl orange (MO,  $M_w = 327 \text{ g mol}^{-1}$ ) and Chrysoidine G (CSG,  $M_w = 249 \text{ g mol}^{-1}$ ).

## Supplementary Tables

**Table S1.** Mechanical properties of PAR-BINOL membranes compared with other typical polymer membranes used in OSN.

Membranes	Young's modulus of the membrane (GPa)		Refs
	Wrinkling method	PFQNM	
PAR-BINOL	-	7.6	This work
PAR-TTSBI	4.8	-	1
CMP	4.0-5.4	6.2-6.7	2
PA	0.4	0.6	
PA	0.3-2.7	-	3
PIM-1	0.8	-	4

**Table S2** Chemical compositions calculated based on the deconvolution O1s peak in the high-resolution XPS spectra of the PAR-BINOL membrane.

O=C-QR (%)	Q=C-OR/COO- (%)	C-Q (%)	$n_{(7,7\text{-OH-BINOL})}/n_{(\text{TMC})}$ in PAR-BINOL layer <sup>a</sup>
23.7	29.8	46.5	1.8

<sup>a</sup>The  $n_{(7,7\text{-OH-BINOL})}/n_{(\text{TMC})}$  in the PAR-BINOL layer was calculated by the following equation:

$k = \frac{3}{4} \times \frac{a+b}{c}$ , where  $k$  is the value of  $n_{(7,7\text{-OH-BINOL})}/n_{(\text{TMC})}$ ,  $a$ ,  $b$  and  $c$  represent the percentages of O=C-QR, C-Q and Q=C-OR/COO, respectively.

**Table S3.** Properties of solvents used for nanofiltration tests.

Name	Molar volume <sup>a</sup> (cm <sup>3</sup> mol <sup>-1</sup> ) at 25 °C	Total Hansen Solubility <sup>a</sup> parameter (MPa <sup>1/2</sup> ) at 25 °C	Viscosity <sup>b</sup> (cP) at 25 °C
Acetone	74.0	19.9	0.31
Acetonitrile	52.6	24.4	0.37
Methanol	40.7	29.6	0.54
THF	81.7	19.4	0.46
DMF	77.0	24.9	0.79
Ethanol	58.5	26.5	1.07
IPA	76.8	23.6	2.04
Toluene	106.8	18.2	0.56

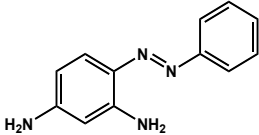
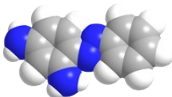
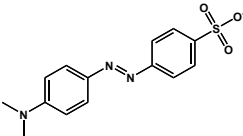
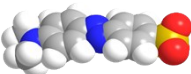
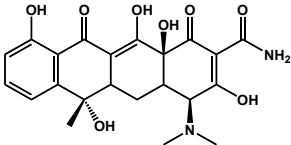
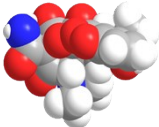
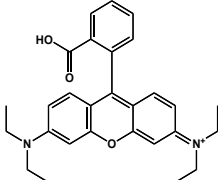

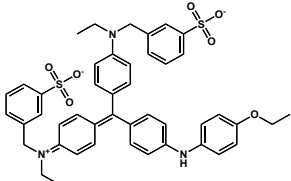
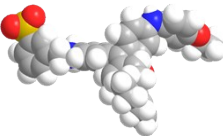
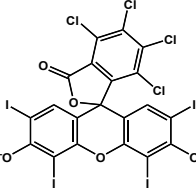
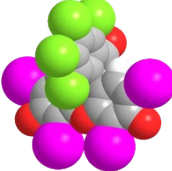
<sup>a</sup> Taken from Hansen Solubility Parameters: A User's Handbook, 2nd Edition, Charles M. Hansen, CRC Press, Boca Raton, FL, 2007.

<sup>b</sup> Taken from CRC Handbook of Chemistry and Physics, 85th Edition, David R. Lide, ed., CRC Press, Boca Raton, FL, 2004.

**Table S4.** Comparison of the solvent permeance of the PAR-BINOL membrane with the reported state-of-the-art OSN membranes in literature.

Support	Nanofilm	Name	Permeance (L m <sup>-2</sup> h <sup>-1</sup> bar <sup>-1</sup> )				Ref.
			Acetone	MeOH	THF	Toluene	
XP84	polyarylate	PAR-BINOL	28.7	9.2	9.0	0.7	This work
PAN	CMP	<i>p</i> -CMP	-	22.5	-	-	7
		<i>m</i> -CMP	-	16.4	-	-	
		<i>o</i> -CMP	-	21.0	-	-	
		<i>p</i> -CMP-OH	-	15.4	-	-	
		<i>p</i> -CMP-OOC2	-	1.43	-	-	
		<i>p</i> -CMP-OOC7	-	1.11	-	-	
XP84	polyarylate	PAR-BHPF	8.4	8.0	4.0	0.3	8
		PAR-TTSBI	7.0	6.0	4.0	2.5	
		PAR-DHAQ	0.2	0.6	0.04	0.01	
		PAR-RES	0.4	0.6	0.04	0.04	
PAN	polyester	β-CD-0.1	-	0.2	-	-	9
		β-CD-0.5	-	1.8	-	-	
		β-CD-1.0	-	5.8	3.2	1.6	
		β-CD-1.5	-	6.1	-	-	
	β-CD-2.0	-	9.6	-	-		
	polyamide	MPDTrip-20	26.5	8.7	7.1	-	10

**Table S5.** Chemical structures, molecular weights and dimensional parameters of various dyes used in this work.

Dyes	M <sub>w</sub> (g mol <sup>-1</sup> )	Chemical structure	3D molecular structure	charge
Chrysoidine G (CSG)	249			+
Methyl orange (MO)	327			-
Tetracycline (TC)	444			0
Rhodamine B (RDB)	479			+
Brilliant Blue R (BBR)	826			-
Rose bengal (RB)	1018			-



**Table S6.** The detailed information about the reported membranes shown in Figure 5c.

Membrane type	Membrane material	Permeance (L m <sup>-2</sup> h <sup>-1</sup> bar <sup>-1</sup> )	Solute M <sub>w</sub> (g mol <sup>-1</sup> )	Rejection (%)	Ref.
Polymeric ISA	Cross-linked PANI	1.4	Styrene oligomers / 236	99	11
Polymeric ISA	Matrimid 5218 (MI) and Polyphenylsulfone (PPSU)	5.0	Sudan II / 276.3	81.0	12
Polymeric ISA	Polyimide (PI)	3.1	Polystyrene oligomers / 236	92.0	13
Polymeric ISA	Polybenzimidazole (PBI)	1.3	Polystyrene / 236	84.0	14
TFN	MOF/PI	15.1	Polystyrene / 236	96.0	15
TFN	GO/PA	8.9	Rhodamine B / 479	98.0	16
TFC	PA / PI	2.4	Styrene oligomers / 236	100.0	17
TFC	PA / CNT / AO	21.7	Rhodamine B / 479	99.8	3
TFC	PAR-TTSBI/PI	7.0	Crystal violet / 408	97.0	8
TFC	PAR-BHPPF/PI	8.4	Crystal violet / 408	98.7	8
TFC	Polyamide-CD/PAN	24.6	Methyl orange / 327	88.0	18
TFC	Freestanding PA / Alumina	49.7	Naphthalene brown / 400	99.9	19
TFC	PAR-BINOL/PI	28.7	Tetracycline / 444	98.2	This work

## Notes and references

1. M. L. Lind, A. K. Ghosh, A. Jawor, X. F. Huang, W. Hou, Y. Yang and E. M. V. Hoek,

- Langmuir*, 2009, **25**, 10139-10145.
2. L. Zhao, P. C. Y. Chang, C. Yen and W. S. W. Ho, *J. Membr. Sci.*, 2013, **425-426**, 1-10.
  3. Z. Zhou, D. Lu, X. Li, L. M. Rehman, A. Roy and Z. Lai, *J. Membr. Sci.*, 2020, **601**, 117932.
  4. A. D. Becke, *Phys. Rev. A*, 1988, **38**, 3098-3100.
  5. C. Lee, W. Yang and R. G. Parr, *Physical Review B*, 1988, **37**, 785-789.
  6. G. A. Petersson and M. A. Al-Laham, *The Journal of Chemical Physics*, 1991, **94**, 6081-6090.
  7. B. Liang, H. Wang, X. Shi, B. Shen, X. He, Z. A. Ghazi, N. A. Khan, H. Sin, A. M. Khattak, L. Li and Z. Tang, *Nat. Chem.*, 2018, **10**, 961-967.
  8. M. F. Jimenez-Solomon, Q. Song, K. E. Jelfs, M. Munoz-Ibanez and A. G. Livingston, *Nat Mater*, 2016, **15**, 760-767.
  9. L. F. Villalobos, T. Huang and K.-V. Peinemann, *Adv. Mater.*, 2017, **29**, 1606641.
  10. Z. Ali, B. S. Ghanem, Y. Wang, F. Pacheco, W. Ogieglo, H. Vovusha, G. Genduso, U. Schwingenschlogl, Y. Han and I. Pinnau, *Adv. Mater.*, 2020, **32**, e2001132.
  11. X. X. Loh, M. Sairam, A. Bismarck, J. H. G. Steinke, A. G. Livingston and K. Li, *J. Membr. Sci.*, 2009, **326**, 635-642.
  12. J. C. Jansen, S. Darvishmanesh, F. Tasselli, F. Bazzarelli, P. Bernardo, E. Tocci, K. Friess, A. Randova, E. Drioli and B. Van der Bruggen, *J. Membr. Sci.*, 2013, **447**, 107-118.
  13. H. Siddique, E. Rundquist, Y. Bhole, L. G. Peeva and A. G. Livingston, *J. Membr. Sci.*, 2014, **452**, 354-366.
  14. G. Szekely, M. F. Jimenez-Solomon, P. Marchetti, J. F. Kim and A. G. Livingston, *Green Chemistry*, 2014, **16**, 4440-4473.
  15. J. Campbell, G. Székely, R. P. Davies, D. C. Braddock and A. G. Livingston, *J. Mater. Chem. A*, 2014, **2**, 9260-9271.
  16. Y. Li, C. Li, S. Li, B. Su, L. Han and B. Mandal, *J. Mater. Chem. A*, 2019, **7**, 13315-13330.
  17. S. Hermans, H. Mariën, C. Van Goethem and I. F. J. Vankelecom, *Current Opinion in Chemical Engineering*, 2015, **8**, 45-54.
  18. T. Huang, T. Puspasari, S. P. Nunes and K. V. Peinemann, *Adv. Funct. Mater.*, 2019, **30**, 1906797.
  19. S. Karan, Z. Jiang and A. G. Livingston, *Science*, 2015, **348**, 1347-1351.